A98-45965

AIAA 98-5142

Challenges and Solutions for Low-Area-Density (LAD) Spacecraft Components

Application to ultra-thin Solar Panel Technology

O. de Weck, W. Hollister
Department of Aeronautics and Astronautics
Massachusetts Institute of Technology
77 Massachusetts Avenue, Cambridge, MA 02139

Defense & Civil Space Programs Conference and Exhibit
von Braun Center, Huntsville, AL
October 28-30 , 1998

AIAA 98-5142

CHALLENGES AND SOLUTIONS FOR LOW-AREA-DENSITY (LAD) SPACECRAFT COMPONENTS APPLICATION TO ULTRA-THIN SOLAR PANEL TECHNOLOGY*

Olivier de Weck[1], Walter Hollister[2]
Department of Aeronautics and Astronautics
Massachusetts Institute of Technology
77 Massachusetts Avenue, Cambridge, MA 02139

Abstract

Spacecraft miniaturization is an important trend in spacecraft design and manufacturing, which has emerged over the last decade. There is however a class of spacecraft components, which can not be scaled down arbitrarily, as they depend on a given surface area A_0 to meet their performance requirements. These components emit or receive RF energy from the space environment and are typically classified as optical mirrors, RF antennas, thermal radiators and solar arrays. When designed as low-area-density (LAD) components, which are thin and ultra-light, they must be stowed during launch and subsequently deployed once on orbit. There are however fundamental limitations to the LAD approach, which arise from the flexible dynamics. It is difficult for components with very low fundamental frequency to maintain a desired surface accuracy in the presence of dynamic disturbances. Potential solutions presented here include active/passive isolation from the noisy spacecraft bus, command shaping and use of embedded smart materials. A large ultra-thin solar array with single axis articulation is used as an illustrative example.

1. Introduction

Spacecraft miniaturization and distributed architectures are two important trends in spacecraft design and manufacturing, which have emerged over the last decade. Due to advances in electronics packaging, light-weight composite materials and micro-mechanical device technology (MEMS), the performance density of spacecraft (e.g. Mbps/kg) is steadily increasing. There is however a class of spacecraft components, which cannot be scaled down accordingly, as they depend on a given surface area A_0 to meet their performance requirements. These components emit or receive RF energy from the space environment and can be classified in the following four categories as: (1) optical mirrors, (2) RF antennas, (3) solar arrays and (4) thermal control system radiators. A reduction in surface area for these components has a direct impact on their performance, assuming constant efficiency. Thus a weight and volume reduction for these items – assuming constant performance – has to focus on a reduction in the third dimension (thickness). This leads to the concept of low-area-density (LAD) components, which are thin and ultra-light and must be stowed during launch and subsequently deployed once on orbit. This paper presents an overview of the challenges that arise from the use of low-area density spacecraft components in the future. Figure 1 shows the MILSTAR communications satellite, which makes use of large, low-area density solar arrays to generate sufficient power for RF communications and spacecraft subsystems supply.

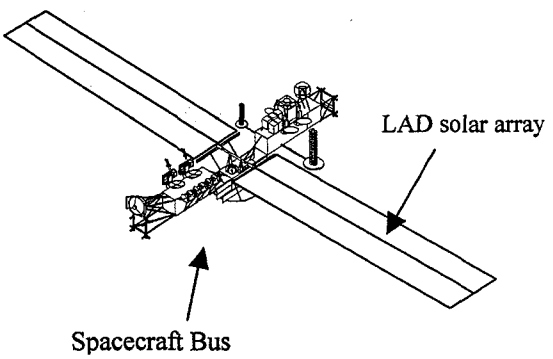

Fig.1 : MILSTAR communications satellite [1]

In order to characterize the challenges for low-areal-density (LAD) components, it is necessary to first define the function and performance metrics, which govern the design of each type of LAD component. Secondly the disturbance environment acting on a component must be characterized. The disturbance analysis propagates these physical

* Student Paper Contribution.
[1] Graduate Research Assistant, Space Systems Laboratory, M.I.T.
[2] Professor, Department of Aeronautics & Astronautics, M.I.T.

disturbances through the component. If it is determined, that if the disturbance is too severe to meet performance, corrective measures have to be taken.

2. Typology of LAD Components

It can be concluded that components, which are appendages to the spacecraft, are usually directly interacting with the space environment. These appendages are clearly candidates for low-area-density components. There is one thing, which all the types of low-area density appendages have in common. They all receive or transmit energy in the form of electromagnetic radiation. The main difference between them is the operating point wavelength and subsequently the accuracy requirements of the surface itself. It is important to note, that the area is merely a collecting or emitting surface, which has to be held to a certain accuracy. The physical laws governing the LAD components' performance are as follows:

Angular resolution of *optical aperture* (~500 nm):

$$\Theta_r(D) = 1.22\,\lambda/D \qquad (2.1)$$

Peak gain in pattern of *RF antenna* (0.001-10m):

$$G(D) = \eta \cdot \frac{\pi^2 f^2 D^2}{c^2} \qquad (2.2)$$

Power generated by *solar array* (250-2000 nm):

$$P_{bol}(A) = P_0 \cdot \eta \cdot A \cdot \cos\Theta \qquad (2.3)$$

Power radiated by *thermal radiator* (1-100 μm):

$$P_{out}(A) = \sigma \cdot T^4 \varepsilon_\lambda \cdot A \qquad (2.4)$$

In all four cases the surface area A or diameter of a circular aperture D, enters directly into the governing equation. If these appendages have made up a significant portion of spacecraft mass and volume in the past, it is due to the massive back frames, truss structures, deployment and actuation mechanisms, which were necessary to ensure the surface accuracy of this class of components. There thus is a demand for a new class of lightweight components, which use active and passive isolation techniques, as well as "smart" sandwich structures with embedded active materials for quasi-static shape control. A reduction in the area-density of components becomes a necessity when the performance requirements become more stringent but mass and volume constraints of present launch vehicles remain constant. Figure 2 shows the trend for reduction in area density for space and land-based telescope primary mirrors and the goals, which have been set by NASA for the next generation space telescope (NGST) primary mirror in particular [2]. Current proposals for the NGST primary mirror range from 14.5 - 22.3 kg/m^2 in terms of the area density.

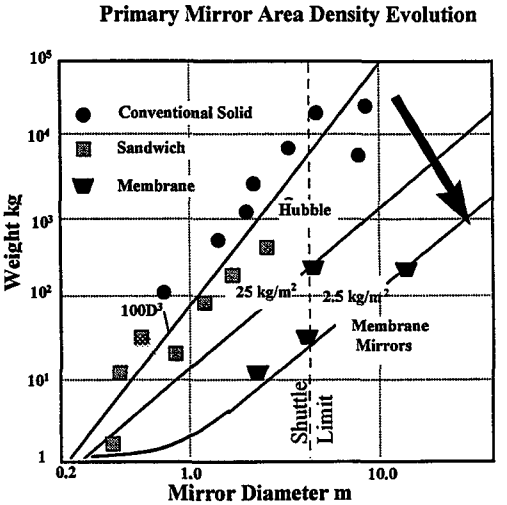

Fig. 2: Trend for area density reduction

3. Performance Modeling

In order for this approach to be successful it is paramount to first exactly understand the function, which each LAD component fulfills and to define appropriate performance metrics. These can later be a basis for the definition of a cost function (e.g. based on H_2 and H_∞ norms), that can be used by a structural controller.

The first step consists of creating a model of the structure, the disturbances and performances. It has to be determined whether the structure can meet the required performances under the influence of the disturbances. This process is shown schematically in figure 3 within the framework of controlled structures technology (CST).

It is necessary to define relevant performance metrics for each low-area-density component, these metrics are different for optical reflectors, RF antennas, thermal radiators or solar arrays, whereby the optical surface precision requirements are the most demanding.

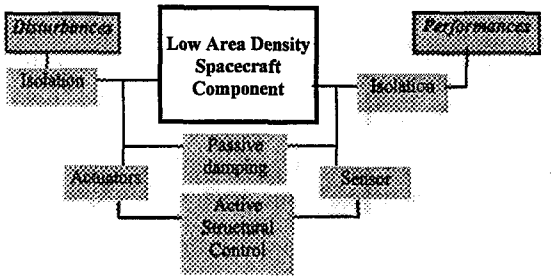

Fig. 3 Analysis and CST- Methodology

In order to assess the performance of various designs, a cost function must be established (e.g. cost per kWh of usable energy from solar panels = cost per unit function). These are generally related to the surface accuracy of the LAD component. The following is a breakdown of typical performance metrics associated with each LAD component:

Thermal Control radiators: Heat flux radiated
- Always pointing to free space
- View factor to rest of spacecraft
- Thermal mass and time constant

Solar Array: Power collected
- Power Loss cost function
- Minimize end-point displacement (bending)
- Minimize torsional twist
- Tracking of input from articulation

RF Antenna: Radiation Pattern
- Peak Gain G_t of main lobe
- Side lobe levels
- Beamwidth Θ
- RMS Surface accuracy

Optical mirrors: Image Quality
- Spherical Aberration
- Coma and Astigmatism
- RMS Surface error **

** RMS surface error:

This is a frequently used performance metric, as it measures the difference between the actual surface and a perfect reference surface and expresses it as a single scalar value. While this number is simple to handle, it does not give any information, which area of the mirror or component surface is contributing the most to the error.

$$e_{RMS} = \frac{\sqrt{(\vec{r}_i - \vec{r}_0)^2}}{N} \qquad (3.1)$$

For NGST the acceptable RMS surface error is a fraction of the wavelength and is expected to be around $e_{RMS} = \lambda/14$, which is around 157 nm for λ=2.2 μm. This is a very stringent requirement. A general statement to be found in the literature is: "The surface accuracy ranges from several percent of wavelength for low frequency applications to a small fraction of wavelength for optical systems" [3]. A surface RMS accuracy of e_{RMS} ~ 1mm is usually sufficient for applications below 15 GHz according to Thomas and Veal [4]. Where the requirements for the surface accuracy of a thermal radiator are not very stringent, they become a major design and cost driver in the case of optical reflectors.

We can model a dynamic performance by determining the following four items:

- Location (where measured, local, distributed)
- Type (displacement, angle, power etc....)
- Amplitude and frequency content

Several performances can be established for a low area-density component. These may then be combined in a single cost function J_z with the help of a weighting matrix R_{zz}. This cost function can be defined in the time domain or in the frequency domain.

4. Disturbance Modeling

An overview of internal (onboard) and external disturbance sources (depending on orbital altitude) acting on LAD components in the space environment is given here. The disturbances, which can affect the structural performance of low-area density components in space, are the ones that exert torques or forces on the LAD components and are shown in a simplified way in Figure 4.

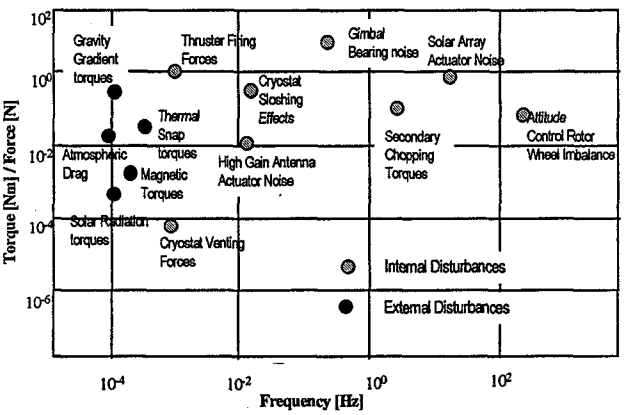

Fig. 4 Typical disturbance characterization (LEO). [5]

It can be seen that the external disturbances are usually quasi-static and have virtually no energy at high frequencies, whereas internal disturbances a have significant high frequency content.

It is now necessary to characterize these disturbances mathematically, in order to use them for our analysis purposes. It is obvious that the external disturbances are mainly a function of the position (altitude) and orientation of the spacecraft, whereas the internal disturbances depend on the design and mode of operation of an individual spacecraft. Regardless of this, the disturbance must be characterized as follows [9]:

- Location
- Type (torque, force, pressure)
- Amplitude and frequency content (PSD)

Generally we can characterize disturbances in the frequency domain or in the time domain, with the primary relationship between the two being the Fourier transform. This has been attempted for one external and one internal disturbance. These results will subsequently be used for the ultra-thin solar array example.

External: Solar Radiation Pressure

The sun emits a flux of electromagnetic energy over a large frequency range. According to Planck's law the peak of the power spectral density corresponds to the surface temperature of the emitting black body (sol: 6000 K). The power received by an area of $1m^2$ at a distance of 1 AU is called the solar constant:

$$P_o = 1358 \pm 5 \text{ W/m}^2 \qquad (4.1)$$

Traditionally the effect of solar radiation pressure on the shape of a spacecraft component had not been considered, because the resulting deflections were negligible. When solar radiation impinges on a non-transmissive low-area density component three kinds of effects may be observed. These are

Absorption

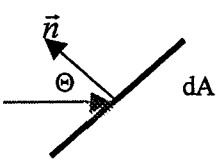

Fig. 5: Solar Radiation Absorption

total absorption, specular reflection and diffuse reflection. A conservative approach is to assume 100% absorption as shown in Figure 5:

$$dF = \alpha_s \cdot \frac{P_o}{c} \cdot \cos\Theta \cdot dA \qquad (4.2)$$

where α_s is the absorptivity of the surface at a given wavelength. For a 3-axis space stabilized spacecraft the relative angle between the surface normal and the incident flux changes only as a function of the mean anomaly and the other orbital elements. An upper bound for the frequency change of the sun incidence angle $\Theta(t)$ in earth orbit is the Schuler period of 84.4 minutes [6]. This results in a frequency of 1.97×10^{-4} Hz. This allows us to model the incident disturbance as a quasi-static distributed force. Dynamically we can model this disturbance as a band-limited white noise with a very low cutoff frequency of $\sim 2.0\times10^{-4}$ Hz. The transfer function between the filtered disturbance d_1 and the white noise disturbance can be written as:

$$G_d(s) = \frac{d_1(s)}{\overline{d_1}(s)} = \frac{\omega_{RO}}{s + \omega_{RO}} \qquad (4.3)$$

The power spectral density of the filtered disturbance can be written as:

$$S_{dd_1} = G_d(j\omega)\, S_{\overline{dd}}\, G_d(-j\omega)^T = \frac{\omega_{RO}^2}{\omega^2 + \omega_{RO}^2} \cdot S_{\overline{dd}} \qquad (4.4)$$

where $S_{\overline{dd}}$ is the power spectrum of the white noise disturbance. The solar pressure can be essentially viewed as a DC disturbance; this however has to be related to the flexible modes of the structure upon which it impinges. An upper bound for the magnitude of the solar pressure disturbance can be assessed by assuming 100% absorption with α_s = 1.0 and a sun incidence angle Θ=0°.

$$dF = \frac{P_o}{c} \cdot dA \qquad (4.5)$$

We thus obtain a maximum magnitude of solar pressure of 4.5×10^{-6} N/m^2.

Internal: Solar Array Actuator Noise

We assume that the solar array is controlled by a one axis actuator, which can rotate the panel about the x-axis. Typically actuator noise is concentrated over a certain frequency range, i.e. it's PSD (power spectral density) is band-limited. The spectrum of the disturbance rolls up at low frequency until a

roll-up frequency ω_{RU}. Then it rolls off again at a frequency of ω_{RO}. The filter or transfer function between the filtered disturbance and white noise is given by:

$$G_{d_2}(s) = \frac{d_2(s)}{\tilde{d}_2(s)} = \frac{\omega_{RO} s}{(s+\omega_{RU})(s+\omega_{RO})} \qquad (4.6)$$

Typically actuators have rotating parts and exhibit internal resonant frequencies. These resonances and their higher harmonics can be identified as peaks in the PSD's, these peaks would be contained in the narrowband disturbance (overbound). Here the power spectrum is the given as:

$$S_{dd_2}(f) = \frac{f^2 f_{RO}^2}{(f^2+f_{RU}^2)(f^2+f_{RO}^2)} S_{\tilde{d}\tilde{d}} \qquad (4.7)$$

Figure 6 shows the amplitude spectrum of the modeled solar array actuator noise, as it will be used in the next section. A peak magnitude of 1 Nm was assumed.

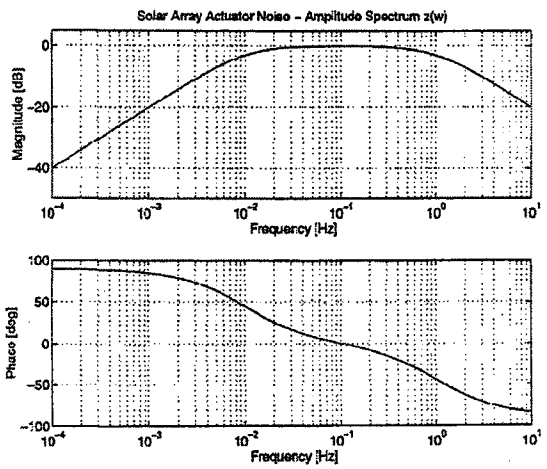

Fig. 6 Solar Array actuator disturbance spectrum

5. Static and Dynamic Analysis

Finally a static and a dynamic model of the low area density component needs to be established in order to see how the disturbances propagate through the structure and to verify if the required performance in terms of a cost function $J_2(\omega)$ can be met.

6. Example: Ultra-Thin Solar Array

This paper uses a specific example from spacecraft subsystem design. An ultra-lightweight rectangular solar array, which is deployed with the help of Bi-Stem technology is shown in figure 7 (area=40m^2).

We consider a planar array, which is a thin flat panel pointed toward the sun. The pointing is achieved with a single axis articulation about the x-axis, which allows the solar array to rotate by and angle Φ, when the solar array actuator exerts a moment $M_x(t)$. This paper assumes that the photovoltaic cells can be manufactured as thin membrane-like materials.

A 2x2cm cross bar represents the attach fitting and provides stability; it is used for deployment of the panel. The thickness of the solar panel has been dimensioned, so that the material is as thin as possible, but does not deflect more than 10% of the solar panel length l at the tip under the influence of the solar pressure (very thin plate). For a first calculation, the solar panel can be modeled as a thin, cantilever beam under uniform loading q. Figure 8 shows the bending line w(x) and maximum deflection f at the tip. The material properties of isotropic aluminum where used, i.e. density ρ = 2700 kg/m^3, Young's Modulus E= 71 GPa and Poisson's ratio ν =0.33.

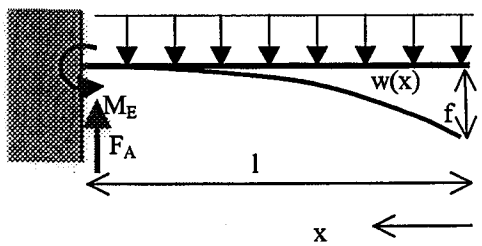

Fig. 8 Cantilever beam approximation

$$w(x) = \frac{ql^4}{24EI_y} \cdot \left[3 - \frac{4x}{l} + \left(\frac{x}{l}\right)^4\right] \qquad (6.1)$$

$$f = \frac{ql^4}{8EI_y} \qquad (6.2)$$

Based on the requirement of less than 10% deflection and a safety factor of 2 (validity of beam approximation), a solar panel thickness of 0.0002 m = 200 μm was chosen. This results in a cross bar mass of 21.6 kg and a solar panel mass of 21.6 kg for a total system mass of 43.2 kg. The area density of this solar panel is thus 1.08 kg/m^2.

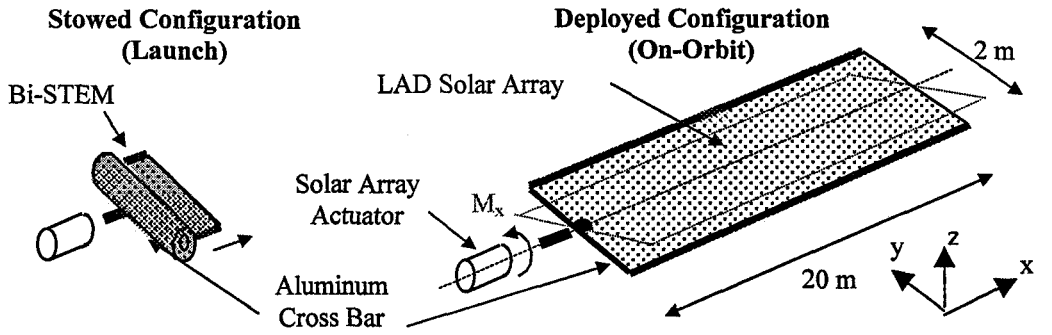

Fig. 7 Design of single-axis articulated LAD solar array with Bi-STEM deployment

The two disturbances which have been considered in this problem are solar radiation pressure d_1, which acts on the entire array surface in negative z direction and solar array actuator noise d_2, which is introduced as a torque in the attach fitting.

The first performance z_1 is the rotation angle θ_x at the tip; this represents a tracking metric, as the tip should track the commanded angle at the input point with a minimal error. The second metric z_2 is related to disturbance rejection. The actuator noise and impulsive inputs are likely to excite the flexible modes of the solar panel, which will cause a power loss as the thin flexible panel starts to oscillate and the projected area A_p is reduced.

We know that the total power collected by the solar panel at the beginning of life (BOL) is given by

$$P_{BOL} = P_o \cdot \eta \cdot A_o \cdot \cos\Theta \tag{6.3}$$

This assumes that the panel is a rigid surface. A power loss due to the flexible dynamics can be calculated with the help of a finite element model. The Power loss coefficient z_2 is defined as the fraction of total power lost due to reductions in the projected area. It is always a value between 0 and 1 and can be calculated as:

$$J_{z2}(\omega) = \left[1 - \frac{dA}{A_o}\sum_{i=1}^{N}\cos(\theta_{i,x})\cdot\cos(\theta_{i,y})\right] \tag{6.4}$$

The power loss function $Jz_2(\omega)$ is defined, to reflect the power which is lost when disturbances (solar array actuator noise, solar pressure) excite the flexible modes of the array.

The deflection angles in the above equation can be obtained from the mode shapes Φ_i of a dynamic model of the array. A performance requirement could be that the cost $J_{z2}(\omega)$ has to be lower than 0.5 over the entire frequency range. Figure 9 shows the definition of the geometry, which defines the power loss coefficient definition.

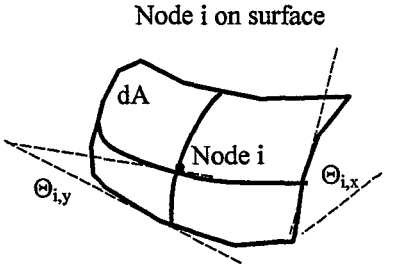

Fig. 9 Power loss function definition
Distorted Panel Surface

In order to asses if the performance metric is met, static and structural dynamic models of the solar panel were created. First the dynamic model was created and a modal analysis for the first 10 flexible modes of the solar panel was conducted. This was done with the help of the ANSYS finite element solver. The solar panel was modeled with 160 4-node bilinear shell elements and a total of 205 nodes.

The basic equation solved in this undamped modal analysis is the classical eigenvalue problem [8]:

$$[K]\phi_i = \omega_i^2[M]\phi_i \tag{6.5}$$

where K and M are the stiffness and mass matrices respectively, Φ_i is the mode shape vector of mode i and ω_i is the natural circular frequency of mode i.

This resulted in a single rigid body mode, which is the rotation about the x-axis. Table 1 gives an overview of the modes and natural frequencies from the modal analysis:

#	Description	Freq. [Hz]
1	Rigid Body Rotation Θx	0.000000
2	First Bending y-axis	0.0004181
3	Second Bending y-axis	0.002617
4	Third Bending y-axis	0.007335
5	First Torsion x-axis	0.009771
6	Fourth Bending y-axis	0.014394
7	Fifth Bending y-axis	0.023842
8	Second Torsion x-axis	0.023962
9	Sixth Bending y-axis	0.035678
10	Third Torsion x-axis	0.039444
11	Seventh Bending y-axis	0.049945

Table 1: Structural Modes of Solar Panel

It can be seen that the fundamental frequency of the panel is 0.0004 Hz, which is extremely low. This frequency is low due to the small bending stiffness. It is however still higher than the rolloff frequency of the solar pressure disturbance d_1. Thus it can be concluded that the solar pressure acts like a static disturbance and will be included only in the static analysis. Figure 10 shows the second torsional mode of the solar panel.

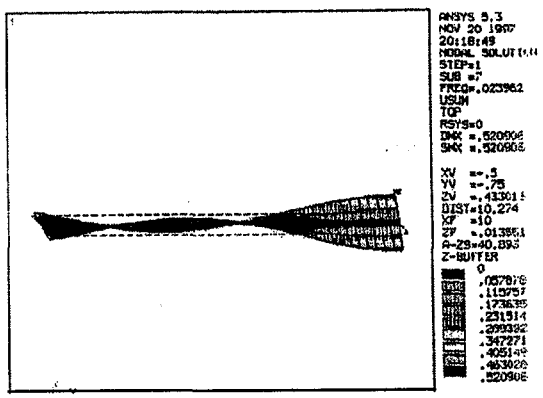

Fig.10 Modeshape for 2nd torsional mode

We are now primarily interested in the transfer function from moment input M_x at the attach point to ϕ_x at the tip point. In order to compute this transfer function a state space representation of the system in second order modal and orthonormal form was obtained. The system in state space representation can be written as follows:

$$\begin{aligned} \dot{x} &= Ax + B_d d \\ z &= C_{zx} x + D_{zd} d \end{aligned} \tag{6.6}$$

where x are the modal orthonormal coordinates, B_d are the disturbance influence coefficients and C_{zd} are the performance influence coefficients. Proportional damping ζ=0.005 was assumed. The disturbance d_2 is the band-limited white noise moment M_x defined in equation (4.6). The performance z_1 is the angle ϕ_x at the tip node. The disturbance to performance transfer function $G_{z1d2}(\omega)$ is shown in figure 11 and is obtained as follows:

$$G_{zd}(\omega) = \frac{z_1(\omega)}{d_2(\omega)} \tag{6.7}$$

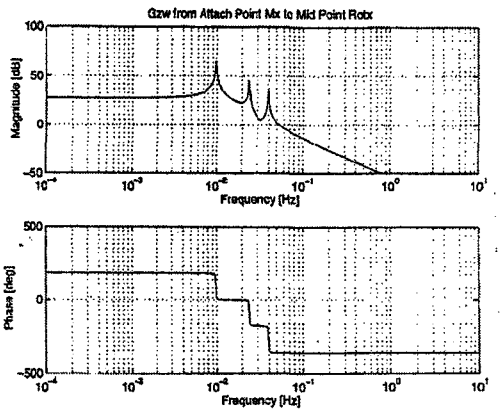

Fig.11 Actuator noise to tip angle transfer function

As expected we only observe the three torsional modes of our model in $G_{z1d2}(\omega)$, the dominant mode being mode 5 just below 0.01 Hz. The bending modes are not observable. Above 0.05 Hz the transfer function rolls off with -40dB/decade. This means that we can not drive the system with fast, impulse-like commands as they will not be transmitted, or alternatively we will excite the flexible modes of the solar panel. The transfer function is typical of non-collocated transfer functions with missing zeros in the pole-zero-pattern. It would be very difficult to close a control loop in this situation due to the large phase losses. This means that for ultra-flexible panels like this one, we have to consider local control, where the sensors and actuators are nearly collocated.

The effect of the disturbance d_2 on the performance z_2 is computed as well. The cost function $J_{z2}(\omega)$ was previously defined and the transfer functions from d_2 to θ_x and θ_y for each node are calculated.

Subsequently the cost function $J_{z2}(\omega)$ is evaluated as defined in equation (6.4). This function is a measure of the power loss due to flexible dynamics. Figure 12 contains the function $J_{z2}(\omega)$ evaluated at each frequency with and without isolation.

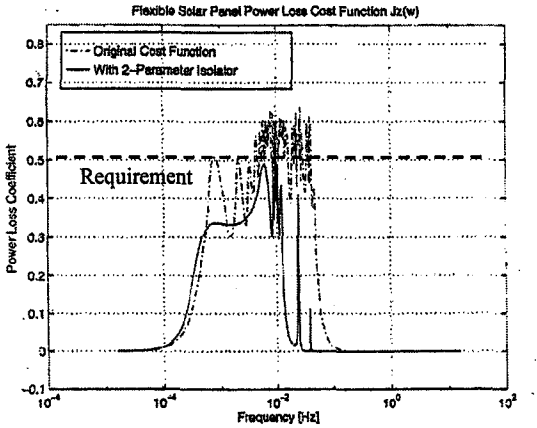

Fig.12: Power loss coefficient $J_{z2}(\omega)$

We can see that the system does not meet the required performance level, which is that $J_{z2}(\omega)$ has to remain below 0.5 at all frequencies. Below 10^{-4} Hz the cost is zero because we are at the lower end of the disturbance spectrum, above 10^{-1} Hz we are also at zero, because the G_{zd} transfer functions rolls off rapidly. The range between 10^{-3} and 10^{-1} Hz characterizes a regime, where the disturbance moment is able to excite the flexible modes of the system and a power loss is experienced.

The ultra-thin solar panel basically acts as a flexible sheet that the solar radiation pressure is able to deflect enough to reduce the collected power. It would be very challenging to control the angular position of the solar panel with the actuator, without exiting the flexible modes of the panel.

7. Potential Solutions for LAD Solar Array

The use of passive isolation between the array and the noisy satellite structure, input shaping for the one-axis articulation input commands and embedded active materials (SMA's) for shape control are investigated as potential solutions.

Isolation from Spacecraft Bus

The disturbance rejection can be accomplished by passively isolating the solar panel from the rest of the spacecraft at higher frequencies. This can be achieved with a passive/active isolator, which is characterized by its transmissibility transfer function $T_\phi(\omega)$. The isolator can be modeled as a torsional spring and dashpot as shown in figure 13.

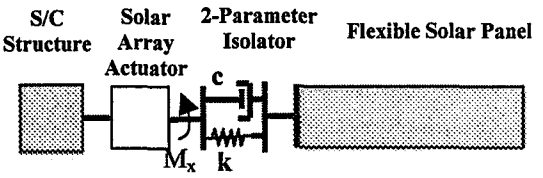

Fig.13: Passive Isolator model for solar array

We choose a 2-parameter passive isolator for simplicity, which meets the following performance requirements:

- Allow Rigid body control (rotation about x-axis) below 0.00055 Hz (T=1800 sec)
- No amplification above 0.001 Hz
- Attenuation of at least 20 dB for the first torsional mode at 0.00977 Hz

We assume that the base (spacecraft structure) is rigid compared to the solar panel. We will first develop the fundamental equations of the 2-parameter isolator and then determine the isolator parameters in order to meet the specification. The moment of inertia of the solar panel about the x-axis can be calculated as:

$$I_{tot} = I_s + I_b = \frac{1}{12} \cdot m \cdot (h^2 + 2b^2) \qquad (6.8)$$

where I_s is the moment of inertia of the panel and I_b is the moment of inertia of the attach fitting. We obtain a value of 14.4 kgm^2 for the entire configuration. The input u is the angle ϕ_u at the actuator end., whereas the output y is the angle ϕ_y at the solar panel end. We can now write the moment equilibrium for the isolator as follows:

$$I_{tot} \cdot \ddot{\varphi}_y = c \cdot (\dot{\varphi}_u - \dot{\varphi}_y) + k \cdot (\varphi_u - \varphi_y) \qquad (6.9)$$

Taking the Laplace transform and solving for the transmissibility we obtain

$$T_\varphi(s) = \frac{cs + k}{I_{tot} s^2 + cs + k} = \frac{2\xi\omega_o + \omega_o^2}{s^2 + 2\xi\omega_o s + \omega_o^2} \qquad (6.10)$$

where ω_o is the natural frequency of the oscillator and ξ is the damping ratio of the oscillator. The transmissibility transfer function crosses the 0 dB line at a frequency of $\sqrt{2}\omega_o$. Assuming a 2.5%

damping in the dashpot, we obtain the following values:

Natural frequency of isolator:

$$\omega_o = \sqrt{\frac{k}{I_{tot}}} = \frac{2\pi}{1800 \cdot \sqrt{2}} = 0.00247 \qquad (6.11)$$

Damping ratio of isolator:

$$\xi = \frac{c}{2\sqrt{kI_{tot}}} = \frac{0.025}{2\sqrt{kI_{tot}}} = 1.563 \qquad (6.12)$$

The torsional spring to be used in the isolator has a value of $k=1.421 \times 10^{-4}$ Nm, which is very soft. This result suggests that active isolation with a controller might me necessary. Theoretically we have achieved attenuation of 24 dB for the first torsional mode. Figure 12 shows the effect of the 2-parameter isolator on the power loss coefficient $J_{z2}(\omega)$.

Isolation can be effective in increasing the performance of low-area density appendages, which are attached to noisy spacecraft structures by acting as a low-pass filter. More advanced isolation schemes with 3-parameter isolators (no amplification) and active isolation with controllers are recommended.

Input Shaping for solar array control

The previous section has raised some valid concerns about the feasibility of rigid body control for the ultra-thin flexible solar panel. We need to rotate the panel fast enough in order to track the sun, which is difficult with an isolator cutoff frequency of 5×10^{-4} Hz, which corresponds to a period of 30 min. An alternative would be to use a technique for rigid body control called input shaping. Input shaping convolves the default moment input with an impulse sequence, so that the panel can be rotated fast, without exciting the first torsional mode of the system [7].

In order to demonstrate the benefits of input shaping, a commanded rigid body rotation of 20° of the solar panel was analyzed. First we create the default moment input $M_o(t)$, secondly we calculate the impulse sequence and convolve the two to create the shaped input and thirdly we analyze the resulting rise time and settling time of the solar panel. The default input $u(t)=M_o(t)$ for a 20° rotation for the rigid body panel can be obtained as follows:

$$\varphi(t) = \int_0^T \dot{\varphi} \cdot dt = \frac{M_o}{2I_{tot}} t^2 + c_1 \qquad (6.13)$$

$$T/2 = \sqrt{\frac{\varphi_o I_{tot}}{M_o}} \qquad (6.14)$$

with the initial angle $c_1=0$, we can solve for the command time T of a square pulse. The panel is accelerated for 50% of the command and decelerated for 50% of the time until it comes to rest at the desired position ϕ_o. In order to shape the input, a three impulse sequence is computed, which is tuned to the first torsional mode ω_5. Assuming a 0.005 damping ratio we can calculate the magnitudes A_i and the time space ΔT of the three pulses as follows [7]:

$$A_1 = \frac{1}{1+2k+k^2} = 0.254 \qquad (6.15)$$

$$A_2 = \frac{2k}{1+2k+k^2} = 0.5 \qquad (6.16)$$

$$A_3 = \frac{k^2}{1+2k+k^2} = 0.246 \qquad (6.17)$$

where the factor k and the spacing ΔT can be completely determined from the following equations:

$$k = e^{\left(\frac{-\xi\pi}{\sqrt{1-\xi^2}}\right)} \qquad (6.18)$$

$$\Delta T = \frac{\pi}{\omega_5 \sqrt{1-\xi^2}} \qquad (6.19)$$

The effects of input shaping are best seen in figure 14. While the unshaped command leads to large oscillations, the shaped input leads to a much shorter settling time.

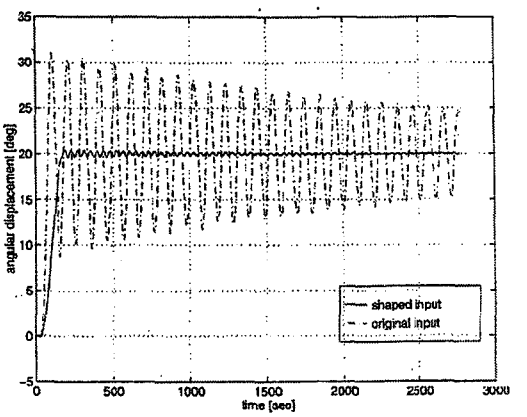

Fig.14: System response for 20° rotation of solar panel

It can be seen that there is a tradeoff between rise and settling times. We sacrifice a small amount of rise time for much shorter settling times with input shaping. With shaping the solar panel has settled down after 275 seconds with the shaped input, when it is still oscillating outside of the ±2% band after 45 minutes, when driven with the unshaped input. It was thus demonstrated, that input shaping is another beneficial way of controlling large flexible space structures. Table 2 summarizes the results for this test case.

Case	Rise [sec]	Settle [sec]
original	31.1	2744.3
shaped	86.6	275.3

Table 2: Improvement in settling time with shaping

Embedded Shape Memory Alloy actuators for quasi-static shape control

The idea presented in this subsection employs SMA actuators in order to correct for the solar panel surface aberration, which is caused by the solar radiation pressure. This technology could also be used to control solar sails and other thin membrane devices in the future. Figure 15 shows the concept of a "smart solar panel" which has embedded SMA actuators to provide quasi-static shape correction. The working principle of the "smart solar cell" idea is as follows:

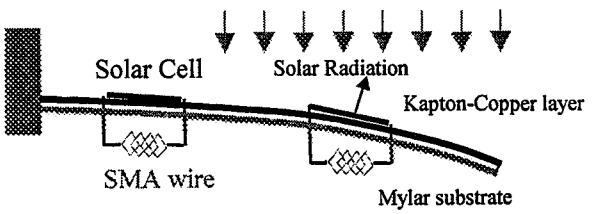

Fig.15: Solar Panel with embedded SMA's

The solar array has a tendency to naturally orient itself toward a light source with this solution. As the angle Θ between the solar cell normal vector and the incident flux becomes smaller, the power, which is generated by the solar cell, increases. This power from a few dedicated cells is directly fed to a SMA actuator, which is embedded above the neutral axis. As the temperature exceeds the phase transformation starts and the actuator contracts. This decreases the curvature even further and again increases the power received by the SMA. Thus the solar panel will be held at a stable equilibrium with all SMA actuators in the fully contracted position.

A further step after using SMA wire actuators, would be an active sandwich membrane structure. An active sandwich structure can meet the requirements for low-area density structures by actuating inside the membrane and thus creating differential strain, which results in a change of curvature. Thus the negative effects of the distributed forces acting as a disturbance in the space environment could be counteracted. Figure 16 shows what the basic layers of such an active sandwich structure for an optical reflector could look like. It will be the subject of future research to show what curvatures and bandwidth can be obtained for different configurations and thermal boundary conditions.

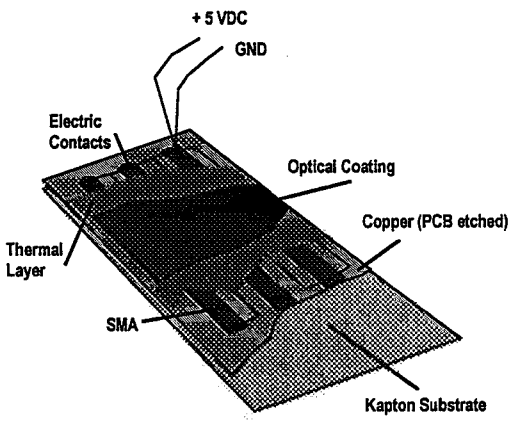

Fig.16: Active membrane sandwich with embedded SMA material

8. Conclusions

It was shown that Low-Area Density (LAD) components offer great opportunities for spacecraft appendages, which depend on a given surface area to meet their performance requirements. There are four types of devices, which are candidates for ultra-thin low-area-density (LAD) components in spacecraft: (1) optical mirrors, (2) RF antennas, (3) solar arrays and (4) thermal control system radiators. The performance of these components is most often related to their surface shape accuracy. The challenge is that ultra-thin components are particularly susceptible to dynamic disturbances.

It was found that disturbances acting on a LAD component can be characterized by type, location, magnitude and frequency content.

In order to successfully implement LAD technology on spacecraft, the following aspects have to be closely examined at the time of spacecraft design and development.

It was shown that it is often necessary to structurally decouple the LAD component from the main spacecraft bus. This can be achieved with passive or active isolators, which act like a low pass filter. The rolloff frequency of the isolator can not be chosen too low or rigid body control will no longer be possible on reasonable time scales. It was shown that input shaping can provide a large improvement, when the shaper is targeted at the dominant flexible modes of the component. Finally active sandwich materials seem promising for controlling low-area density components in the future. This will require a decentralized control architecture, as the pole-zero-patterns of LAD components are not conducive for controlling the structure if the sensors and actuators are non-collocated.

Furthermore the deployment aspect of low-area density structures represents a challenge, which was not addressed in this research.

9. References

[1] Hughes Space and Communications, " Product Overview", Space Clip Art, 1996

[2] NGST Preliminary Design, Presentation to Project Office, NASA Goddard Space Flight Center, 1996

[3] Hedgepeth, J.M., "Accuracy potentials for large space antenna reflectors with passive structures", Journal of Spacecraft, 19 (3), pages 211-217, 1982

[4] Thomas, M., Veal G., " Highly accurate inflatable reflectors", AFRPL, TR-84-021, 1984

[5] Source: Zeiders, Ultima, Symposium on Optical Systems Concepts and Technology for NGST, MSFC, 1996

[6] Larson, Wertz, "Space Mission Analysis and Design", Second Edition, Microcosm Inc. 1992

[7] Campbell M. , Input Shaping, Course notes 16.243

[8] ANSYS, Version 5.3 User Manual, Chapter Structural Analyses, 3.3. Modal Analysis

[9] Crawley E., Campbell M., Chapter 7, "Performance and Disturbance Modeling", Draft, 4/2/1997

Nomenclature

A	surface area	[m^2]
A_o	nominal surface area	[m^2]
c	speed of light	[m/sec]
d_1	solar pressure disturbance	[N/Hz]
d_2	actuator noise disturbance	[Nm/Hz]
D	diameter	[m]
dF	differential Force exerted	[N]
E	Young's Modulus	[Pa]
f	frequency	[Hz]
I_b	area moment of inertia	[m^4]
J_z	performance cost function	[-]
K	global stiffness matrix	[N/m]
L	length of solar array	[m]
M	global mass matrix	[kg]
M_x	actuator control torque	[Nm]
N	number of surface measurements	[-]
P_o	solar constant at 1 AU	[W/m^2]
q	uniform pressure loading	[N/m]
R_o	reference surface	[m]
R_i	actual surface	[m]
R_{zz}	performance weighting matrix	[-]
T	surface temperature	[K]
α_s	absorptivity	[-]
λ	wavelength	[m]
ε_λ	emissivity at wavelength	[-]
η	efficiency	[-]
ϕ	solar array rotation angle	[rad]
θ	angle between surface normal and flux	[rad]
σ	Stefan-Boltzmann constant	[W/m^2K^4]
ω_{RO}	rolloff frequency	[rad/sec]
ω_{RU}	rollup frequency	[rad/sec]